Laser and Particle Beams (2009), *27*, 511–520. Printed in the USA.

doi:10.1017/S0263034609990243

Electrical explosion process and amorphous structure of carbon fibers under high-density current pulse igniting intense electron-beam accelerator

LIMIN LI,[1] LIE LIU,[1] GUOXIN CHENG,[1] LEI CHANG,[1] HONG WAN,[2] AND JIANCHUN WEN[1]

[1]College of Photoelectric Science and Engineering, National University of Defense Technology, Changsha, People's Republic of China
[2]Department of Material Engineering and Applied Chemistry, National University of Defense Technology, Changsha, People's Republic of China

(Received 12 April 2009; Accepted 18 June 2009)

Abstract

The development of pulsed power technology, particularly for inductive energy storage, promotes the extensive discussions of electrical explosion process in high energy density. This paper presents the electrical-explosion behavior of carbon fibers subjected to about 20 kA, ~5 μs high-density current pulse igniting an intense electron beam accelerator. After electrical explosion, and surface rupture, submicron particles, fibrillar and strip-shaped structures were observed, experimentally supporting the microstructure model (skin-core heterogeneity) of carbon fiber. Interestingly, the start and turn-off of the current were followed by radiation pulses with different intensities. It was found that the radiation was focused on the explosion stage which was characterized by an oscillating current. The instabilities of plasma produced during the explosion process play an important role in the microstructure changes of carbon fibers and the radiation generation.

Keywords: Electrical explosion; Electron beam accelerator; High energy density; Pulse radiation; Submicron structure

1. INTRODUCTION

In the past few years, there has been considerable interest in electrical wire explosion as a phenomenon first described in the 18th century. In the electrical explosion process, the physical state of wire changes abruptly as a result of intense energy deliberation when the wire carries a pulsed current of high density (10^6–10^9 A/cm^2) (Sedoi *et al.*, 1999). Thus, the rapid heating of the exploded wire allows an investigation of the physical properties of materials and, particularly, its phase transformations going through the all states from condensed matter to plasma. Furthermore, thermodynamic data in the liquid state, and evaluations of the critical point resulted from traditional thermophysical measurements, were obtained with wire explosion experiments (Lomonosov, 2007). Electrical wire explosion has been widely used in various applications, such as high-voltage pulsed power system (Mao *et al.*, 2009; Yatsui *et al.*, 2005; Zou *et al.*, 2006; Koyama *et al.*, 2006; Chen *et al.*, 2008), nanopowder production (Sindhu *et al.*, 2008; Jiang & Yatsui, 1998), Z-pinch experiments (Hammer & Sinars, 2001; Clardi *et al.*, 2002), warm-dense-matter studies (Saski *et al.*, 2006), and X-ray sources (Liu *et al.*, 2008*b*, 2008*c*; Hong *et al.*, 2009; Kasperczuk *et al.*, 2009; Krása *et al.*, 2009). For the production of nanoparticles in which the wires are embedded in gases, the vapor generated by electrical explosion process is cooled by colliding with the gas molecules, forming nanoparticles from the condensed vapor. Particularly for high-voltage pulsed power system, exploded wires are generally utilized in opening switches modulating the accelerating pulse of high-current electron beam diodes (Liu *et al.*, 2007, 2009; Tarasenko *et al.*, 2008; Huang *et al.*, 2008; Burdovitsin & Oks, 2008). This type of switch is called an electrically explosive opening switch (EEOS) that are suitable for high-voltage pulse generators based on inductive energy accumulators. The EEOS, as a replacement of the large volume transmission line, can directly generate a high-voltage pulse, which enables the simple and compact construction of pulse generators (Grigoryev *et al.*, 1997). The inductive energy accumulator usage is considered in the high-voltage pulse generator, mainly as a result of the possibility to obtain the

Address correspondence and reprint requests to: Limin Li, College of Photoelectric Science and Engineering, National University of Defense Technology, Changsha 410073, People's Republic of China. E-mail: newages1979@yahoo.com.cn

high densities of the accumulated energy at a relatively low specific density (Chuvatin *et al.*, 2006; Zhang *et al.*, 2008).

Actually, the explosion of wires occurs, if subjected to high-density current, subsequently turning off the circuit. This rapidly excites a high voltage across the diode load, thus enabling the generation of high-current pulsed electron beam from explosive emission cathodes (Li *et al.*, 2007, 2009*a*, 2009*d*). The turn-off time of EEOS depends on the wire length, wire material, and ambient mediums (different gases) (Sedoi *et al.*, 1999). The mechanisms governing the electrical wire explosion are mainly attributed to the thermal instability due to Joule heating by high-density current (Oreshkin, 2008). During the electrical explosion process, a number of phenomena, including instabilities, shunting discharges, and stratification, develop which make the underlying mechanism significantly complicated (Sedoi *et al.*, 1999). It has been found that the initial wire dynamics may affect the development of the instabilities, the formation of precursor plasmas on the axis (Hammer & Sinars, 2001; Politov *et al.*, 2000). However, the exact physical mechanisms of electrical explosion process are far fully characterized.

Considerable experimental investigations were carried out on the emission characteristics of carbon fibers as field emitters under the external large electric field (Li *et al.*, 2008, 2009*b*, 2009*e*). However, discussions on the property of carbon fibers, subjected to the electrical explosion process, are scarce in the literature. The aim of the present work is to investigate the behavior of carbon fibers by passing high current through them. Additionally, we observed the pulse radiation going with the operation of EEOS. To understand the behavior of carbon fibers under the electrical explosion process, we present experimental investigations, and some possible explanations for these phenomena.

2. EXPERIMENTAL SETUP

The experimental system consists of an initial energy supplier (capacitance bank), a trigger switch, a transformer with a coupling coefficient of 0.89, an EEOS, a sharpening spark-gap switch as main switch, and a high-current electron beam diode as load (see Fig. 1). When the charged capacitance bank has a 45 kV voltage, the voltage across the trigger switch is up to 55 kV (see Fig. 2). Then a negative high-voltage pulse is loaded on the trigger electrode, and the breakdown between the trigger and input electrodes occurs due to the significant electric field enhancement. This is accompanied by the secondary discharge between the trigger and output electrodes. Thus the trigger switch rapidly turns on, and the capacitance bank discharges, forming a pulsed high current in the primary circuit of the transformer. Meanwhile, the EEOS delivers a pulsed high current in the branch circuit of the secondary side of the transformer. Figure 3a presents the EEOS with an organic glass plate, macromolecule rods (polytetrafluor ethylene), and two arrays of carbon-fiber wires arranged in "Z" shape.

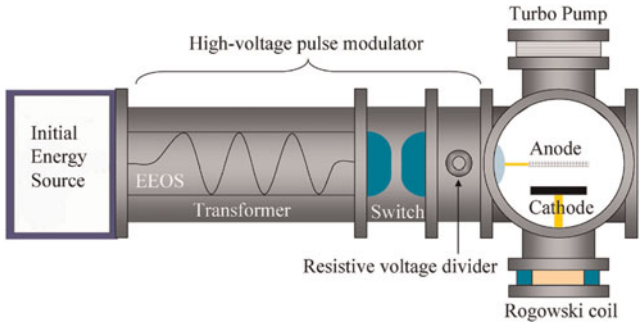

Fig. 1. (Color online) Diagram of an intense electron-beam accelerator with inductive energy storage. The accelerator consists of the initial energy source, EEOS, coaxial transformer, main switch, and vacuum diode. The vacuum vessel shows the cathode mount, cathode, anode, and vacuum pump. The anode-cathode gap can be changed by moving the shaft upon which the cathode is mounted.

These wires are positioned at the two sides of the plate, each side having eight wires. Each wire, 0.5 mm in diameter and 770 mm in length, contains about 100 carbon fibers. Polyacrylonitrile (PAN)-based carbon fibers with a diameter of about 5–7 μm, purchased from Wuxi carbon fiber company (People's Republic of China), were used. The plate is placed in a cylindrical chamber made of macromolecule, 20 cm in diameter and 50 cm in length, as shown in Figure 3b. This chamber was filled with 4 atm. SF_6 or N_2 that acts to inhibit arcing. The start and end of these fiber wires are connected with a copper rod, respectively. Further, the copper rod at the end is electrically connected with the transformer, and the wall of the chamber is grounded. Once the pulsed high current passes the EEOS, the electrical wire explosion occurs as the temperature grows fast due to the Joule heating. That is, the EEOS turns off, and an over 400 kV voltage forms across the main switch, leading to the self-breakdown, and further sharpening the accelerating pulse. This provides sufficient electric field to the cathode to emit the high-current electron beam. A Rogowski coil is used to measure the EEOS current with the voltage monitored by a resistive divider. The pulse radiation is detected by an antenna that is place at a distance of 20 m from the EEOS. The radiation signal

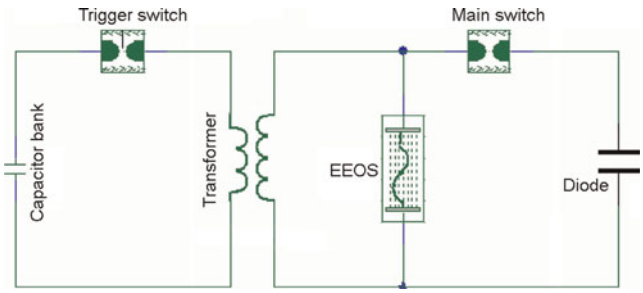

Fig. 2. (Color online) Equivalent circuit of the intense electron-beam accelerator. Capacitor bank: capacitance 18 μF, trigger switch: breakdown voltage 45 kV, transformer: initial inductance 5.64 μH and secondary inductance 52 μH, main switch: breakdown voltage 400 kV.

https://doi.org/10.1017/S0263034609990243 Published online by Cambridge University Press

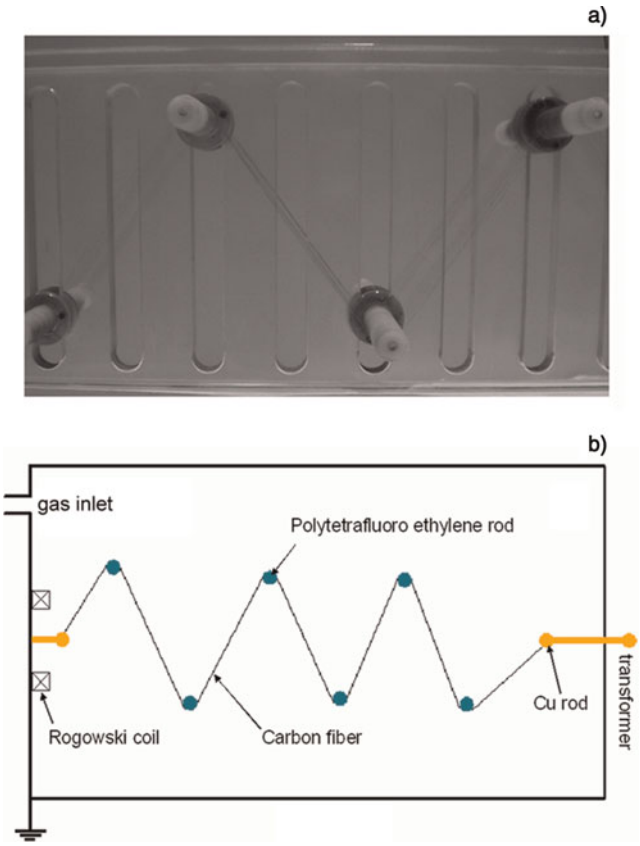

Fig. 3. (Color online) (**a**) An organic glass plate, macromolecule rods, and two arrays of carbon fibers arranged in "Z" shape. (**b**) A drawing of the experimental chamber in which the fibers are tested.

is transmitted through a coaxial attenuator, and a coaxial cable to a Tek 3052B oscilloscope (sampling rate of 5Gs/s).

3. RESULTS AND DISCUSSIONS

To understand further the electrical explosion process, the typical current pulse of the carbon fibers is shown in Figure 4. The maximum current reached up to 19.8 kA, and the pulse duration was about 4.7 μs. Thus, the current density of each fiber bundle was estimated to be 6.3×10^5 A/cm^2, assuming each wire current to be equal. Based on the general notions about the state of the exploded wire material (Mao *et al.*, 2009), the process can be divided into three stages, namely, the heating stage, phase changed stage, and the explosion stage (see Fig. 4). These stages are significantly different in the terms of the degree of changes in the density and resistivity of electrically exploded wires. In the first stage, the absorbed contaminants and epoxy on the fiber surface were liberated as the high current heats. Meanwhile, the resistance of carbon fibers increased in this stage. However, the current had a higher increasing rate than that of resistance, finally leading to an increase in the current amplitude. When the carbon fiber is heated to the evaporation point (at the end of stage I), its resistance

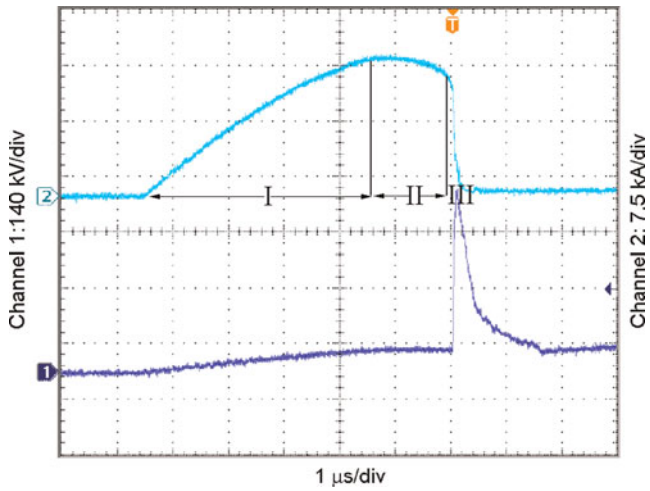

Fig. 4. (Color online) Typical waveform of high current pulse (Channel 1) passing through the carbon fibers, and the current development can be divided into three stages: I heating stage, II phase change stage, and III explosion stage. The diode voltage is also shown (Channel 2).

substantially limits the rate of current rise. Indeed, the heating stage lasted from the onset of current passage to the evaporation, about 3.2 μs. During the second stage, the current reached its maximum value without the significant changes in the amplitude, and it lasted about 1.3 μs. In this stage, the energy delivered to the carbon fiber is sufficiently high to excite atoms, destroy chemical bond, and vaporize the fiber materials. Finally, in the third stage, the electrical conductivity of the material starts rapidly falling, indicating the beginning of the electrical explosion of carbon fiber. Here the vaporized gases expand in an explosive manner, which is accompanied by an abrupt increase in the resistance. This explosion process occurred within about 200 ns, and finally the current was cut-off. In the last stage, the fiber materials are exploded into ionized neutral gases, with the formation of plasma. The over 400 kV, ~350 ns diode voltage pulse synchronously appeared in this stage. It should be noted that the rising side of voltage pulse is erected by the main switch. The formation of a high-voltage pulse also indicates the electrical explosion of fiber wires. Throughout the whole current pulse, the material goes through several states: the solid state, a mixture of phases, phase transitions, the gaseous state, and plasma. Here the division of three stages is based on the changes in the material state. The initial stage covers the heating of carbon fiber in the solid state until the onset of vaporization. As this takes place the fiber density changes insignificantly. Next is the phase transition to the gaseous state and plasma, and considerable energy is required for latent heat of phase change. In the second stage, the current was around the maximum value for 1.3 μs, demonstrating the possibility of phase transitions. Finally, the fiber explosion occurs, which is accompanied by an abrupt increase in resistance due to the decrease in the density of the fiber material resulting from its expansion. There are many physical effects that may

https://doi.org/10.1017/S0263034609990243 Published online by Cambridge University Press

influence this explosion process. These are the skin effect, the plasma instabilities, the thermal stress, the discharge along the surface of carbon fibers, etc, (Mao *et al.*, 2009). The specific energy at the initial point of explosion and the total input energy at the end of the explosion both depend on the rate of heating and on the density of the environment. It should be pointed out that the above three stages are roughly divided in time. Based on the circuit in Figure 2, the simulation result of EEOS current pulse is shown in Figure 5. One can see that the current pulse reaches its maximum value, ~20 kA, with a risetime of ~2.8 μs, and the EEOS is cut-off within <200 ns at the end of the current pulse. The main difference between experimental and simulated results is in the second stage, namely, the time interval for the EEOS current to keep its maximum value. Clearly, this interval in simulation is smaller than that of the experimental result. This is mainly due to the fact that the physical processes in the phase transitions are not fully characterized by the circuit simulation. Overall, the simulation result is in good agreement with the experimental observations in Figure 4.

Figure 6 shows the surface morphology images of carbon fibers before and after high current pulsed discharge. Here the carbon fibers carried a high current pulse with a maximum value of about 20 kA. Figure 6a shows the original carbon fibers with a typical diameter of 5–7 μm. It can be seen that the original carbon fibers exhibit a great number of striations on the surfaces of monofilaments along the fiber axis, which is typical for PAN-based carbon fibers (Liu *et al.*, 2008*a*). Figure 6b presents the particles and broken fibers, as two typical productions. If the electrically exploded conductor is a metal wire, the productions by electrical explosion process are no other than particles, which has been discussed widely (Jiang & Yatsui, 1998; Sindhu *et al.*, 2008). However, in the case of carbon fiber, the particles and broken fibers coexisted, implying the electrical explosion process is incomplete. That is, the carbon fibers are not exploded into particles completely. It should be pointed out that all of carbon fibers participate in the electrical explosion process. The nature behind the incomplete explosion stems from the difference between carbon fiber and metal in terms of the electrical properties. Under the application of a high current pulse, the break and rupture of carbon fibers occurred (see Fig. 6c). The cross-sectional morphology of the carbon fibers after high current pulsed discharge is shown in Figure 6d. It was found that the diameter of carbon fiber increased up to >10 μm. Also, such an increase in fiber diameter was clearly observed from Figure 6c, and enough tests have been performed to ensure that the change in diameter is not due to statistical variation from fiber manufacturing. This indicates the structure relaxation of carbon fiber due to the joule heating of high current. Moreover, there existed a lot of valleys with a width of hundreds of nanometers, which is absent in Figure 6a. These valleys had a typical depth of <1 μm (see Figs 6c and 6d), that is, the surface rupture happened in the region close to the surface of carbon fibers. This likely demonstrates that the skin effect plays an important role in the electrical explosion process. Here the surface rupture of carbon fibers also shows the energy deposition of pulsed high current. Further, the energy is mainly focused on the surface of carbon fibers. Most notably, many submicron particles were attached on the surface of carbon fibers, as shown in Figure 6c. These particles may be liberated from inside materials of carbon fibers or sprayed from neighboring fibers during high current pulsed discharge. After high current pulsed discharge, the surface morphology of carbon fibers was characterized by irregular valleys and ridges with several hundreds of nanometers. It should be noted that water is absorbed on the fiber surface. The surface rupture of carbon fiber is mostly due to the large thermal stress, under the application of high current pulse. The absorbed water is evaporated from the fiber surface by fast Joule heating initially in the current pulse. Thus, water has little effects on the formation of these cracks, since water is only limited to the fiber surface. Indeed the evaporation process is initiated from the fiber surface due to the skin effect, and develops toward the inside. The skin depth can be calculated as $\delta = (2\rho/\omega\mu)^{1/2}$, where ρ is the resistivity of carbon fiber, ω is the current frequency, and μ is the magnetic conductivity. Here the fundamental frequency is $2\pi \times 10^5$ Hz, for a current pulse of about 5 μs. At $\mu = 1$ and $\rho = 10^{-6}$–10^{-5} $\Omega \cdot$ m for carbon fiber, the skin depth $\delta > 1.7$ μm is obtained. This indicates the current is limited to the surface region initially in the pulse, namely, the surface flashover plays an important role in the initial stage. However, the skin depth increased as the pulse proceeded due to a fast increase in the resistivity of carbon fiber and, as a result, the conduction of current is in volume and not merely a surface flashover. As the materials are vaporized, the effective area of carbon fibers for conducting current sharply reduces, leading to a rapid increase in the resistance.

To conceive the process of electrical explosion affecting the surface of carbon fiber, it is necessary to analyze the microstructure of carbon fiber. Its microstructure is characterized by the skin-core heterogeneity (Manders, 1978). It has been understood that carbon fiber consists of three layers:

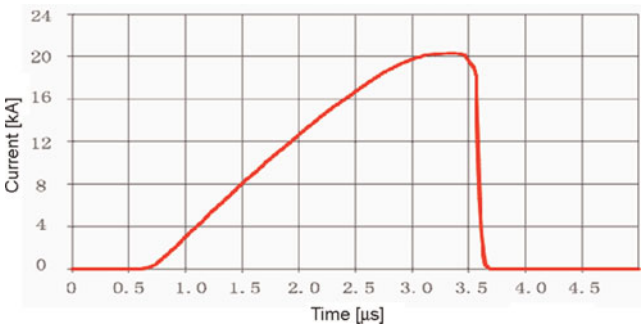

Fig. 5. (Color online) Simulation waveform of EEOS current pulse based on the circuit in Figure 2.

https://doi.org/10.1017/S0263034609990243 Published online by Cambridge University Press

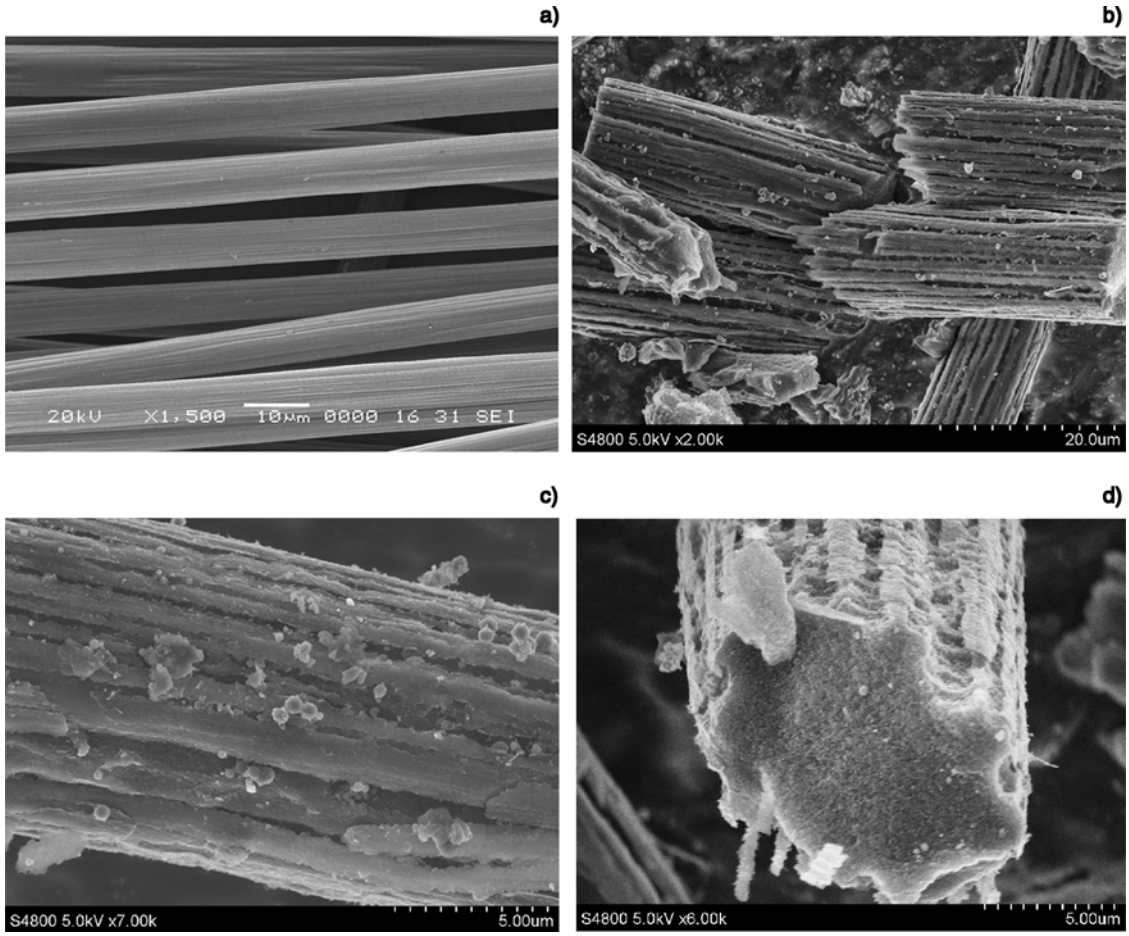

Fig. 6. SEM images of carbon fibers: (**a**) side view of original carbon fibers, (**b**) broken fibers and particles, (**c**) surface rupture of fibers, and (**d**) cross section.

the surface, crust, and the core. The surface is parallel to the axis of fiber, and the medium crust layer includes carbon granules that are randomly distributed. Although the surface of the fiber is its most oriented part, it contains both crystal edges coming out at the surface and defect-free main atomic planes. High energy marginal atoms are interconnected by sp^2 bonds and can actively chemisorb oxygen. Surface atoms of the main planes, which constitute structure of ideal graphite lattice interact through most weak σ-bonds and thus have a considerably weaker surface activity. Besides, fibrillar microstructure, micropores, crystallite edges, microinclusions, cracks which are nuclei of destruction can also be discovered on the surface. Just due to these defects on fiber surface, the electrical explosion occurs easily at sites where these defects reside. The surface rupture of carbon fiber, subjected to the high-density current pulse, to some extent shows the microstructure of carbon fiber.

Figures 7a and 7b, respectively, show the submicron particles with two typical shapes (square and near-sphere), generated by high current pulsed discharge of carbon fibers. Besides, the square particles in Figure 7a got together, while the near-sphere particles in Figure 7b show a scattered pattern. It is an important problem that the broken fibers and submicron particles were generated together. This is mainly due to the fact that the electrical explosion is initiated from the local sites along the fiber (Jiang & Yatsui, 1998). Namely, there exist discrete explosion centers or points along the carbon fibers during the electrical explosion process. The liberation of inside and/or outside materials of carbon fibers is the major source of these particles. Thus, these particles may be generated at the explosion centers. However, why these particles had two different shapes is not fully understood, and it seems likely that the square and near-sphere particles come from the inside and surface of carbon fibers, respectively. On the surface of carbon fibers, the near-sphere particles are generated mainly by the evaporation and deposition of carbon due to the fast heating of high current pulse. Moreover, these near-sphere particles can also be observed on the ruptured surface of carbon fibers in Figure 6c. Due to the skin effect, the major part of pulse current is centered on the surface region. Thus, the energy is mainly deposited on the surface. However, the deposited energy is not sufficient to achieve the evaporation of carbon completely. It is possible to produce square particles seemingly connected each other. Also, the

https://doi.org/10.1017/S0263034609990243 Published online by Cambridge University Press

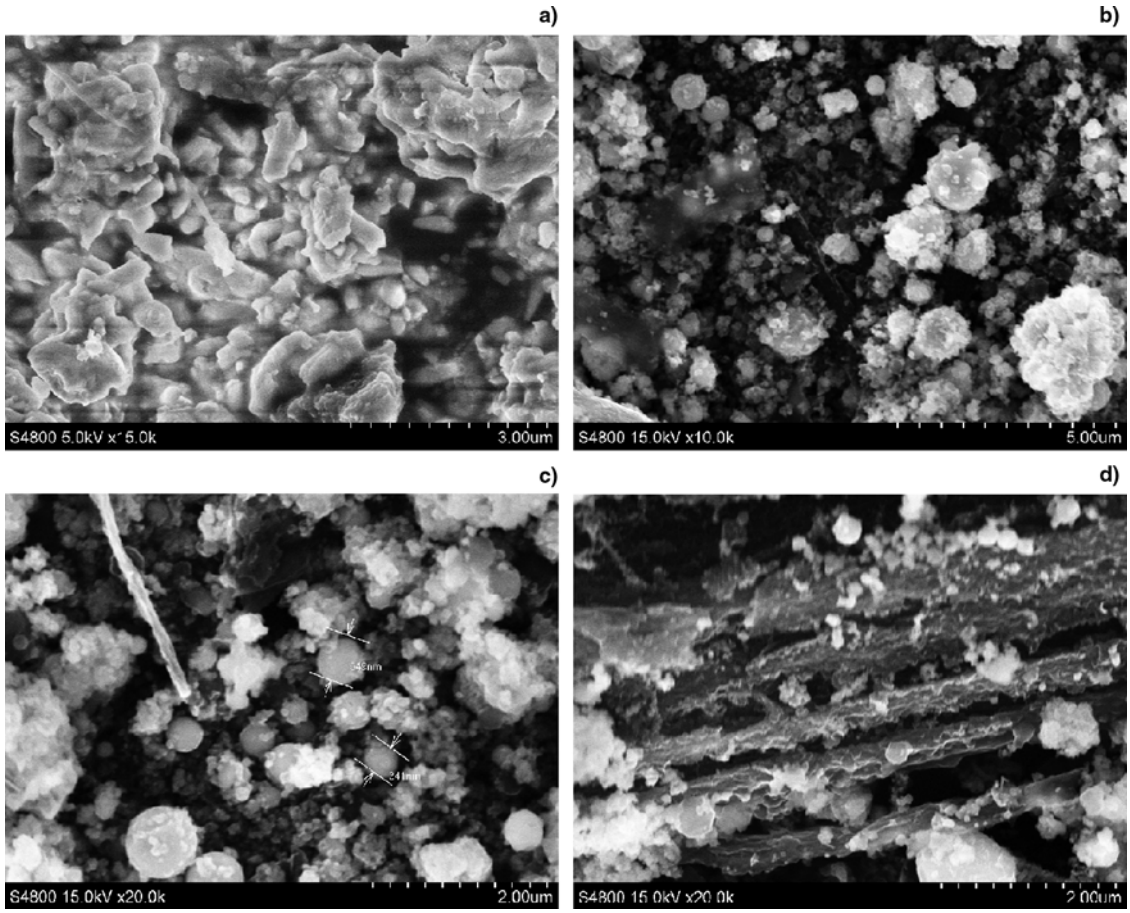

Fig. 7. Submicron particles with two typical shapes: (**a**) square and (**b**) near-sphere. Fibrillar (**c**) and strip-shaped (**d**) structures are also generated.

agglomeration of the square particles may stem from electrostatics or Van der Waals forces. Therefore, such two types of particles demonstrate the energy distribution on the cross section of carbon fibers. Most notably, the fibrillar and strip-shaped structures are also generated, as shown in Figures 7c and 7d. In Figure 7d, one can see that the near-sphere particles were attached on the strip-shaped structures, without the square particles. It seems likely that the strip-shaped structures come from the surface layers of carbon fiber.

The entire process, which involves heating and vaporization, followed by condensation of the vapor molecules, is activated by deposition of the appropriate amount of energy into the electrically exploded wires. After the evaporation of fiber, the plasma-deposited vapor-liquid mixture begins to expand in the medium due to the large differences in the temperature and pressure between the evaporated conductor vapor and the ambient gas. The vapor particles formed during the vaporization process get cooled by collisions with inert-gas atoms in the ambient. Thus, the temperature of the vapor particles rapidly gets reduced to a value much lower than the boiling point of the metal. The size of the vapor particles in the expanding vapor is $s_p = 2\sigma(T)/(p_v - p_s)$ (Sindhu *et al.*, 2008), where $\sigma(T) = \sigma_0\ [1 - (T/T_c)]$ is the surface tension as function of temperature T, T_c is the critical temperature, p_v is the vapor pressure, and p_s is the saturation pressure. Here, it should be pointed out that the filled gases are utilized as ambient medium, mainly to avoid the oxidation of particles. Also, the observation of these particles indicated a large amount of energy liberated by the electrical explosion process in a short period. Such a fast process holds many energy-liberation forms, e.g., thermal diffusion, light emission, and shock wave. Of course, the electromagnetic pulse radiation is one of them.

Interestingly, the onset and turn-off of the EEOS current are accompanied by pulse radiations, indicating the simultaneity between them, as shown in Figure 8. Further, the second pulse had a higher intensity than that of the first pulse. If the attenuation of radiation signals is increased, the first pulse radiation will not be detected. There exist two factors involved in this phenomenon, namely, the switch turn-on/off and current changing ratio. The former determines whether the pulse radiation appears or not. That is, once the EEOS current rapidly changes, it is followed by the pulse radiation. The current changing ratio is responsible for the difference in the radiation intensity between the two pulses. Indeed, the fastest change in the current is in the explosion stage. That is, the electrical wire explosion process induced the second pulse radiation with a higher intensity.

https://doi.org/10.1017/S0263034609990243 Published online by Cambridge University Press

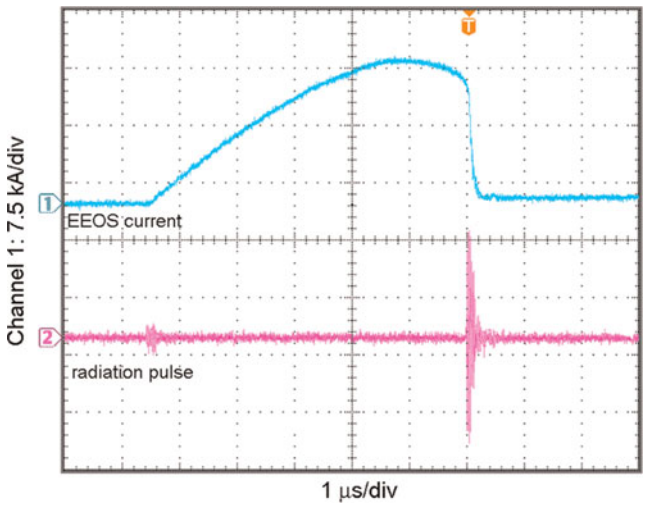

Fig. 8. (Color online) Typical waveforms of the EEOS current (Channel 1) and, with the pulse radiation (Channel 2). Here the ambient medium of electrically exploded wires is SF_6.

Thus, the attention is focused on the underlying nature of the radiation generation during the electrical wire explosion process.

Figure 9 shows the radiation signal, generated by electrical wire explosion, and its spectrum. Here the initial point of time corresponds to the end of stage II, namely, the start of the electrical explosion. At the gain coefficient of the antenna for the dominant frequency $G = 2.4$ dB, i.e., 1.74, the effective receiving area was determined to be $A_e = G\lambda^2/4\pi = 2.3\ m^2$. Taking the attenuator 36 dB, measurement cable 1 dB, and antenna reflection 3 dB into account, the receiving power of antenna P was about 1800 W. Thus the average power density in a distance of 20 m from the EEOS can be estimated to be $P/A_e = 772\ W/m^2$. From Figure 9b, one can see that the radiation frequency was in the range of 40–150 MHz with a dominant frequency of about 75 MHz. Additionally, it is necessary to know the variation of the radiation frequency as a function of time, and this is done using a sliding fast fourier transform (FFT). Figure 9c presents the sliding FFT analysis of radiation signal. Here the regions with high intensity frequencies are blue with low intensity or little red (color online only). Clearly, the radiation starts from the time corresponding to the peak of diode voltage. Also, the radiation frequency of 75 MHz occurred at this time. This further indicates about 75 MHz radiation component was generated at the onset of electrical explosion.

Since the current changing rate is responsible for the intensity of pulse radiation, the falling edge of EEOS current should be taken into account. Figure 10 shows the current for the EEOS cut-off, the spectrum of its difference, and the corresponding sliding FFT. Surprisingly, the difference of EEOS current has a spectrum similar to the spectrum of pulse duration (see Fig. 10b). One can see that the dominant frequency is around 72 MHz. Besides, this dominant frequency appears when the electrical explosion begins, as

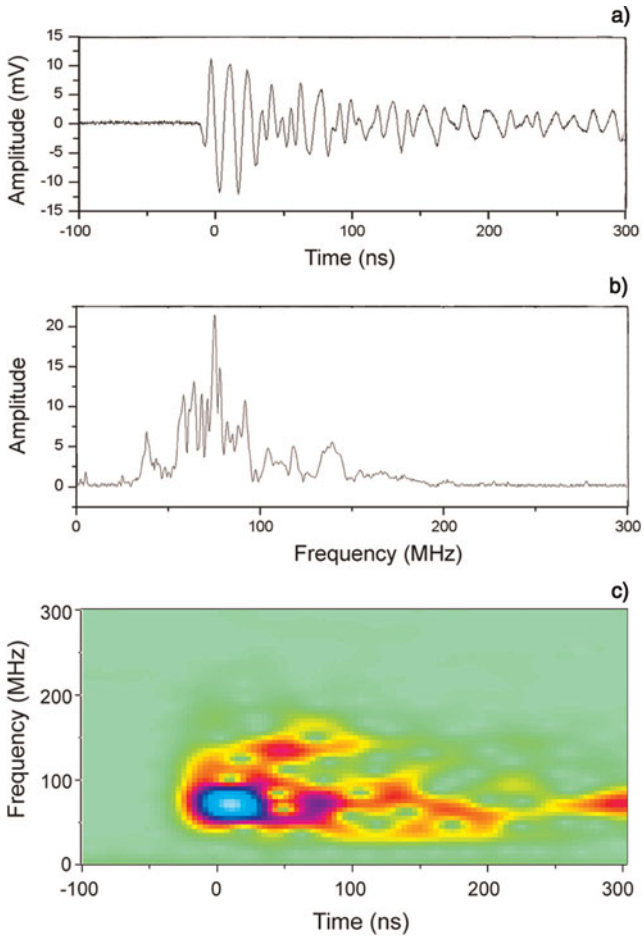

Fig. 9. (Color online) Radiation pulse (**a**) generated by electrical wire explosion and its spectrum (**b**). Sliding FFT of the radiation signal illustrates the evolution of radiation frequency as a function of time (**c**). Here the ambient medium of electrically exploded wires is SF_6.

seen from Figure 10c. Therefore, the pulse radiation arises from the rapid oscillation of the cutoff current.

Figure 11 presents the typical waveforms of the EEOS current, the pulse radiation and its spectrum in the case of N_2 ambient medium. The EEOS current slightly changed as compared with the case of SF_6. Notably, two radiation pulses appeared, respectively, at the start and cut-off of EEOS current, with the second being many times higher than the first in terms of the pulse intensity. That is, the pulse radiation is focused on the stage of electrical explosion. Also, this further supports the experimental observation in the case of SF_6 ambient medium. Thus, the electrical explosion determines the pulse radiation. Further, one can see that the dominant frequency was around 42.5 MHz, lower than that for SF_6. Therefore, the filled medium plays an important role in the radiation frequency.

Since the plasma is produced in the electrical explosion process, the dynamic behavior of plasma is also an important issue in understanding the surface modification and submicron-particle formation of carbon fibers. The electrical explosion process of carbon fibers is initiated from the local

https://doi.org/10.1017/S0263034609990243 Published online by Cambridge University Press

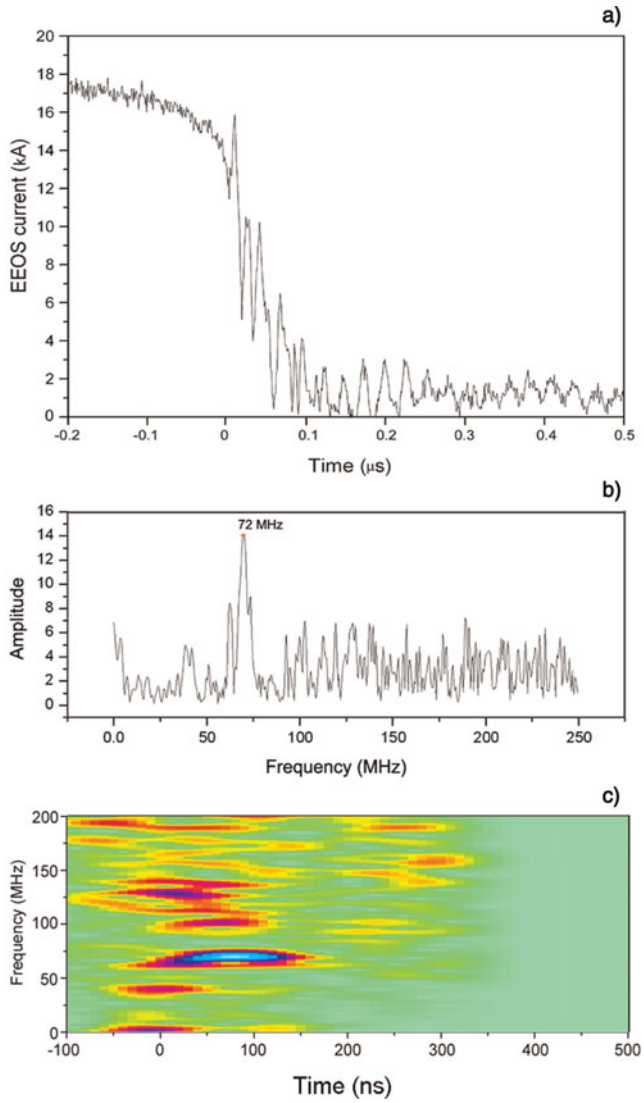

Fig. 10. (Color online) Typical waveform of the cutoff current of electrically exploded wires (**a**), its difference spectrum (**b**), and the corresponding sliding FFT (**c**). Here the ambient medium of electrically exploded wires is SF_6.

sites. This is related to the fact that the changes in the resistivity of carbon fibers strongly depend on the injected current. Generally, the distribution of injected current is nonuniform along the fiber length. This will lead to the nonuniform axial resistivity of carbon fibers. Since the electrical explosion is attributed to the Joule heating, fiber explosion first appears at the site with a higher resistivity. Meanwhile, the local explosion is followed by the formation of plasma gas. Once a high current pulse goes through the carbon fiber, a strong magnetic field, circling the fiber, will be generated. Here the magnetic field interacts with the current, forming a self-magnetic field force ($\mathbf{J} \times \mathbf{B}$). Thus, the plasma will be limited in a region close to the fiber. However, the thermal stress of plasma gases inhibits the above effect. Namely, there is a dynamic equilibrium between the self-magnetic field force and the plasma thermal stress, determining the development of plasma gas.

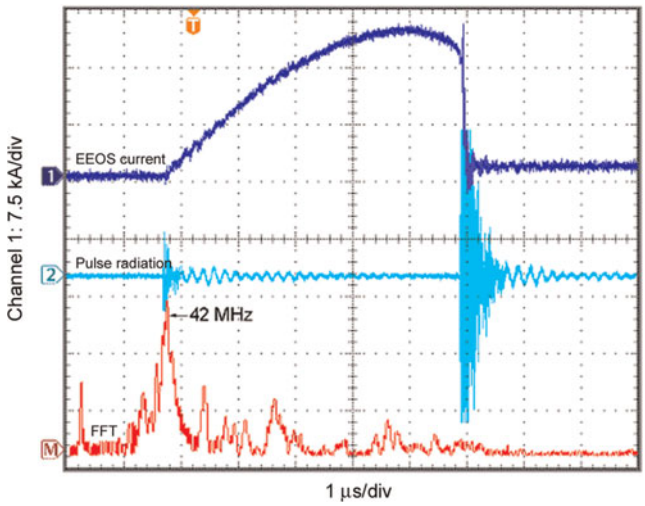

Fig. 11. (Color online) Typical waveforms of the EEOS current (Channel 1), with the pulse radiation (Channel 2) and its spectrum (the lowest). Here the ambient medium of electrically exploded wires is N_2.

Based on the steady-state solution of the magneto-hydrodynamic equations, in the case of isotropic pressure, the radius of the plasma column is given by $r = (i/\pi)\sqrt{\mu/4p}$, where i is the current going through the carbon fiber, μ is the plasma magnetic conductivity, and p is the plasma pressure (Sindhu *et al.*, 2008). Clearly, the radius of the plasma gas column is closely related to the discharge current and plasma pressure.

From Figure 10a, one can see that the current exhibited a significant oscillation, even a variation of several kiloamperes initially in the explosion process. Surprisingly, after a huge drop, the current can still recover its most amplitude rapidly. However, this is only a short-lived process that the current decreased from about 16 kA to about 5 kA within several nanoseconds. The oscillation behavior of the current is closely related to the instabilities of plasma. The changes in the current or the shock wave generated by fiber explosion likely gives rise to some disturbances of plasma (e.g., filamentation or sausage instabilities), thus forming plasma gases with diverse shapes (Jiang & Yatsui, 1998). As a result, the fiber resistance changes sharply, allowing an exchange between increase and decrease of EEOS current. The generation of plasma, during the explosion process, can enhance current conduction, leading to a fast increase in the pulse current for a short time. However, the self-magnetic field force can not stop the plasma expansion, and finally the current is cut-off. Indeed, the plasma expansion comes at the cost of a decrease in plasma temperature, that is, the heating of plasma by current can not compensate synchronously such a temperature change.

4. CONCLUSIONS

In summary, the property of carbon fibers was investigated under the application of about 20 kA, ~5 μs high current

https://doi.org/10.1017/S0263034609990243 Published online by Cambridge University Press

pulse. After high current pulsed discharge, a remarkable increase in the fiber diameter was observed. This indicates the energy deposition of high current pulse. Indeed, subjected to a high current pulse, the fiber surface was ruptured with valleys of several hundreds of nanometers, and some particles were deposited on the surface. Most notably, the surface rupture appeared in the region of about 1 μm depth close to the fiber surface. This phenomenon can be attributed to the skin effect, forming a nonuniform current distribution. Interestingly, the submicron particles with two typical shapes (near-sphere and square), and fibrillar and strip-shaped structures were generated. The evolution of high current pulse can be divided into three stages, namely, the heating stage, phase change stage, and explosion stage. Additionally, the current in the explosion stage showed a significant oscillation, stemming from the plasma instabilities.

Further, the start and turn-off of the EEOS were accompanied by pulse radiation. The radiation was focused on the turn-off of the EEOS or the explosion stage. In this stage, the oscillating current may be responsible for the formation of pulse radiation. Besides, the filled gases in the chamber had effects on the pulse radiation. However, the generation of pulse radiation, in spite of different ambient mediums, mainly occurred in the electrical explosion process. Overall, the microstructure changes and the formation of pulse radiation may be related to the development of plasma produced in the electrical explosion process.

ACKNOWLEDGMENT

This work was supported by the National High Technology Research and Development Program of China.

REFERENCES

Burdovitsin, V.A. & Oks, E.M. (2008). Fore-vacuum plasma-cathode electron sources. *Laser Part. Beams* **26**, 619–635.

Chen, Z.L., Unick, C., Vafaei-Najafabadi, N., Tsui, Y.Y., Fedosejevs, R., Naseri, N., Masson-Laborde, P.-E. & Rozmus, W. (2008). Quasi-monoenergetic electron beams generated from 7 TW laser pulses in N2 and He gas targets. *Laser Part. Beams* **26**, 147–155.

Chuvatin, A.S., Kokshenev, V.A., Aranchuk, L.E., Huet, D., Kurmaev, N.E. & Fursov, F.I. (2006). Laser plasma interaction in copper nano-particle targets. *Laser Part. Beams* **24**, 395–401.

Clardi, A., Lebedev, S.V., Chittenden, J.P. & Bland, S.N. (2002). Modeling of supersonic jet formation in conical wire array Z-pinches. *Laser Part. Beams* **20**, 255–261.

Grigoryev, V.P., Koval, T.V. & Potashev, A.G. (1997). Influence of radiation on a virtual cathode triode impedance and voltage pulse. *SPIE* **3158**, 254–259.

Hammer, D.A. & Sinars, D.B. (2001). Single-wire explosion experiments relevant to the initial stages of wire array z pinches. *Laser Part. Beams* **19**, 377–391.

Hong, W., He, Y., Wen, T., Du, H., Teng, J., Qing, X., Huang, Z., Huang, W., Liu, H., Wang, X., Huang, X., Zhu, Q., Ding, Y. & Peng, H. (2009). Spatial and temporal characteristics of X-ray emission from hot plasma driven by a relativistic femtosecond laser pulse. *Laser Part. Beams* **27**, 19–26.

Huang, Y., Duan, X., Lan, X., Tan, Z., Wang, N., Tang, X. & He, Y. (2008). Time-dependent neutral-plasma isothermal expansions into a vacuum. *Laser Part. Beams* **26**, 671–675.

Jiang, W. & Yatsui, K. (1998). Pulsed wire discharge for nanosize powder synthesis. *IEEE Trans. Plasma Sci.* **26**, 1498–1501.

Kasperczuk, A., Pisarczyk, T., Nicolai, P., Stenz, C., Tikhonchuk, V., Kalal, M., Ullschmied, J., Krousky, E., Masek, K., Pfeifer, M., Rohlena, K., Skala, J., Klir, D., Kravarik, J., Kubes, P. & Pisarczyk, P. (2009). Investigations of plasma jet interaction with ambient gases by multi-frame interferometric and X-ray pinhole camera systems. *Laser Part. Beams* **27**, 115–122.

Koyama, K., Adachi, M., Miura, E., Kato, S., Masuda, S., Watanabe, T., Ogata, A. & Tanimoto, M. (2006). Monoenergetic electron beam generation from a laser-plasma accelerator. *Laser Part. Beams* **24**, 95–100.

Krása, J., Velyhan, A., Jungwirth, K., Krouský, E., Láska, L., Rohlena, K., Pfeifer, M. & Ullschmied, J. (2009). Repetitive outbursts of fast carbon and fluorine ions from sub-nanosecond laser-produced plasma. *Laser Part. Beams* **27**, 171–178.

Li, L.M., Liu, L., Chang, L., Wan, H., Wen, J. & Liu, Y. (2009*a*). Characteristics of polymer velvet as field emitters under high-current pulsed discharge. *Appl. Surf. Sci.* **255**, 4563–4568.

Li, L.M., Liu, L., Wan, H., Zhang, J., Wen, J. & Liu, Y. (2009*b*). Plasma-induced evolution behavior of space-charge-limited current for multiple-needle cathodes. *Plasma Sources Sci. Technol.* **18**, 015011.

Li, L.M., Liu, L. & Wen, J. (2007). Microstructure changes of cathodes after electron emission in high power diodes. *J. Phys. D* **40**, 5338–5343.

Li, L.M., Liu, L., Wen, J. & Liu, Y. (2009*c*). Effects of CsI coating of carbon fiber cathodes on the microwave emission from a triode virtual cathode oscillator. *IEEE Trans. Plasma Sci.* **37**, 15–22.

Li, L.M., Liu, L., Wen, J., Men, T. & Liu, Y. (2008). An intense-current electron beam source with low-level plasma formation. *J. Phys. D: Appl. Phys.* **41**, 125201.

Li, L.M., Liu, L., Xu, Q., Chang, L., Wan, H. & Wen, J. (2009*d*). Propagation of individual plasma spots on cathode surface by high-current discharge process. *Phys. Lett. A* **373**, 1165–1169.

Li, L.M., Liu, L., Xu, Q., Chen, G., Chang, L., Wan, H. & Wen, J. (2009*e*). Relativistic electron beam source with uniform high-density emitters by pulsed power generators. *Laser Part. Beams* **27**, 335–344.

Liu, J.L., Cheng, X.B., Qian, B.L., Ge, B., Zhang, J.D. & Wang, X.X. (2009). Study on strip spiral Blumlein line for the pulsed forming line of intense electron-beam accelerators. *Laser Part. Beams* **27**, 95–102.

Liu, J.L., Yin, Y., Ge, B., Zhan, T.W., Chen, X.B. & Feng, J.H. (2007). An electron-beam accelerator based on spiral water PFL. *Laser Part. Beams* **25**, 593–599.

Liu, L., Song, Y.J., Fu, H.J., Jiang, Z.X., Zhang, X.Z., Wu, L.N. & Huang, Y.D. (2008*a*). The effect of interphase modification on carbon fiber/polyarylacetylene resin composites. *Appl. Surf. Sci.* **254**, 5342–5347.

Liu, R., Zou, X., Wang, X., He, L. & Zeng, N. (2008*b*). X-pinch experiments with pulsed power generator (PPG-1) at Tsinghua University. *Laser Part. Beams* **26**, 33–36.

Liu, R., Zou, X., Wang, X., Zeng, N. & He, L. (2008*c*). X-ray emission from an X-pinch and its applications. *Laser Part. Beams* **26**, 455–460.

Lomonosov, I.V. (2007). Multi-phase equation of state for aluminum. *Laser Part. Beams* **25**, 567–584.

Manders, P.W. (1978). Carbon fiber structure by electrolytic etching. *Nat*. **271**, 142–143.

Mao, Z., Zou, X., Wang, X., Liu, X. & Jiang, W. (2009). Circuit simulation of the behavior of exploding wires for nano-powder production. *Laser Part. Beams* **27**, 49–55.

Oreshkin, V.I. (2008). Thermal instability during an electrical wire explosion. *Phys. Plasmas* **15**, 092103.

Politov, V.Y., Potapov, A.V. & Antonova, L.V. (2000). About diagnostics of Z-pinches hot points. *Laser Part. Beams* **18**, 291–296.

Saski, T., Yano, Y., Nakajima, M., Kawamura, T. & Horioka, K. (2006). Warm-dense-matter studies using pulse-powered wire discharges in water. *Laser Part. Beams* **24**, 371–380.

Sedoi, V.S., Mesyats, G.A., Oreshkin, V.I., Valevich, V.V. & Chemezova, L.I. (1999). The current density and the specific energy input in fast electrical explosion. *IEEE Trans. Plasma Sci*. **27**, 845–849.

Sindhu, T.K., Sarathi, R. & Chakravarthy, S.R. (2008). Understanding nanoparticle formation by a wire explosion process through experimental and modelling studies. *Nanotechnology* **19**, 025703.

Tarasenko, V.F., Baksht, E.H., Burachenko, A.G., Kostyrya, I.D., Lomaev, M.I. & Rybka, D.V. (2008). Supershort electron beam from air filled diode at atmospheric pressure. *Laser Part. Beams* **26**, 605–617.

Yatsui, K., Shimiya, K., Masugata, K., Shigeta, M. & Shibata, K. (2005). Characteristics of pulsed power generator by versatile inductive voltage adder. *Laser Part. Beams* **23**, 573–581.

Zhang, Y., Tang, J., Huang, J., Qiu, A., Guan, Z. & Wang, X. (2008). The application of flash-over switch in high energy fluence diode. *Laser Part. Beams* **26**, 213–216.

Zou, X.B., Liu, R., Zeng, N.G., Han, M., Yuan, J.Q., Wang, X.X. & Zhnag, G.X. (2006). A pulsed power generator for x-pinch experiments. *Laser Part. Beams* **24**, 503–509.

https://doi.org/10.1017/S0263034609990243 Published online by Cambridge University Press